**Supporting Information**

**Corresponding author's email: prack@utk.edu**

# Inert Gas Enhanced Laser-Assisted Purification of Platinum Electron-Beam-Induced Deposits

**Michael G. Stanford[1], Brett B. Lewis[1], Joo Hyon Noh[1], Jason D. Fowlkes[1,2], and Philip D. Rack[1,2*]**

1) Materials Science and Engineering Department, University of Tennessee, Knoxville, TN 37996, USA

2) Nanofabrication Research Laboratory, Center for Nanophase Materials Sciences, Oak Ridge National Laboratory, Oak Ridge, TN 37381, USA

## Purification reaction with localized and non-localized gas flow

$H_2O$ is an abundant residual gas which has been shown to purify Pt EBID deposits[1]. Here we use inert Ar gas flow to enhance the surface diffusion of residual $H_2O$ molecules to facilitate the laser assisted purification reaction with the $PtC_5$ EBID patterns. The source of the residual $H_2O$ which contributes toward purification reactions may be (1) outgassing of chamber walls, (2) outgassing of the substrate, or (3) from contamination in the inert gas line. Figure S1a compares the EDS spectra of $PtC_5$ deposits which were laser annealed under flux of localized and non-localized Ar gas, with 10 μs and 1% duty cycle laser conditions. Clearly, the localized gas flux was more effective in purifying the deposits, as indicated by a significant reduction in the carbon content. Figure S1b displays RGA spectra which show that the chamber gas composition was very similar for the two laser anneals. Inert gas flow localized to the substrate as well as non-localized flow should have similar effect at facilitating $H_2O$ outgassing at the chamber walls. Minimal purification with non-localized Ar flux rules out enhanced contribution from $H_2O$ from the chamber wall. Figure 3 indicates that the inert gas line has minimal $H_2O$ contamination. We therefore conclude that the localized Ar gas flux supplied from the GIS needle facilitates the localized enhanced surface diffusion of $H_2O$ from the substrate.

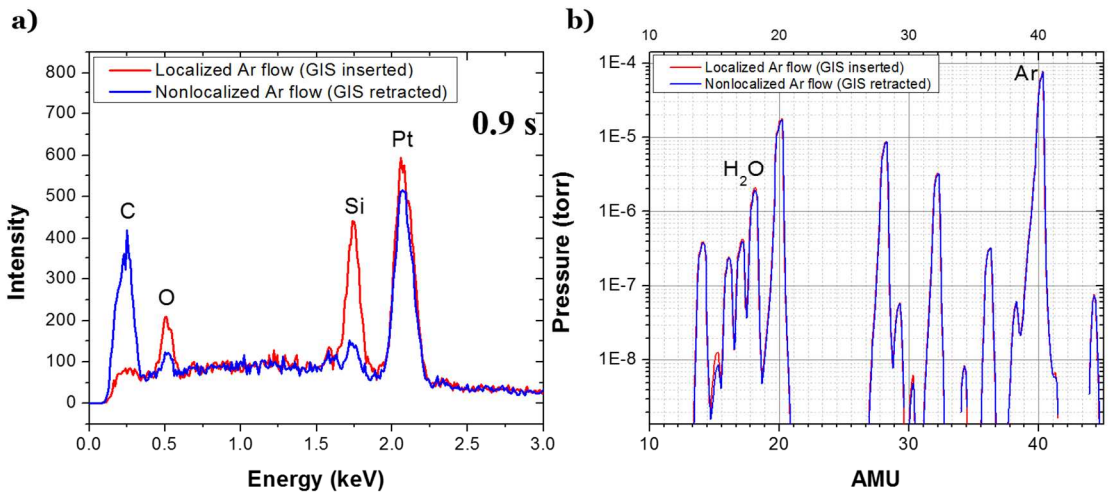


**Figure S1.** (a) EDS spectra of Pt EBID deposits which were annealed with 10 us and 1% duty cycle laser conditions for a cumulative laser exposure time of 0.9 s. Spectra shown include a deposit annealed under localized Ar flow and a deposit annealed under non-localized Ar gas flow. The partial pressure of the Ar flow was approximately 1.0E-6 mbar for both anneals. (b) RGA spectra showing the chamber gases species present during both of the anneal processes.

**Reactive gas assisted LAEBID synchronization**

Figure S2 illustrates the synchronization of the LAEBID process for 500 nm x 500 nm deposits for a single LAEBID pass, where a single pass consists of an electron beam raster sequence in which each pixel is serially addressed. Specifically, the schematics reported here are for LAEBID which utilized 10 µs laser pulse width at 1%, 3%, and 6% duty cycle. The electron beam was set to raster from the top left of the pattern to the bottom right, with an x- and y-axis pixel spacing of 13.55 nm and a 10 µs dwell time. In the schematic, the blue boxes represent pixels when the electron beam and laser pulses are irradiating simultaneously. All other white boxes represent pixels where the electron beam is on and no laser irradiation occurs. Importantly, during laser irradiation (blue pixels), the laser spot size is large enough that the entire deposit is simultaneously irradiated. The ratio of laser pulse on-time per LAEBID pass, as well as other experimental parameters for the LAEBID processes are reported in Table S1. In this table, highlighted carbon content denotes that the deposit was compromised by laser induced chemical vapor deposition (LCVD), which deposits Pt in the entire laser spot size. Therefore, the most successful LAEBID conditions not convoluted with the LCVD reaction (10 µs, 6% DC) were

able to deposit a pattern with only ~25 % of the carbon content of a standard EBID deposit (~55.7 at% carbon). It is also clear that there is a trend between Laser/Ebeam "on" time and the carbon content of the deposit. Longer laser exposures, or the $H_2O$ reactive gas anneal 2$^{nd}$ half-reaction, enhance the final purity of the deposit. A large enhancement in material purity (just 25% of carbon compared to standard EBID deposits) was able to be realized using the LAEBID process, and deposits exhibited high fidelity and shape retention.

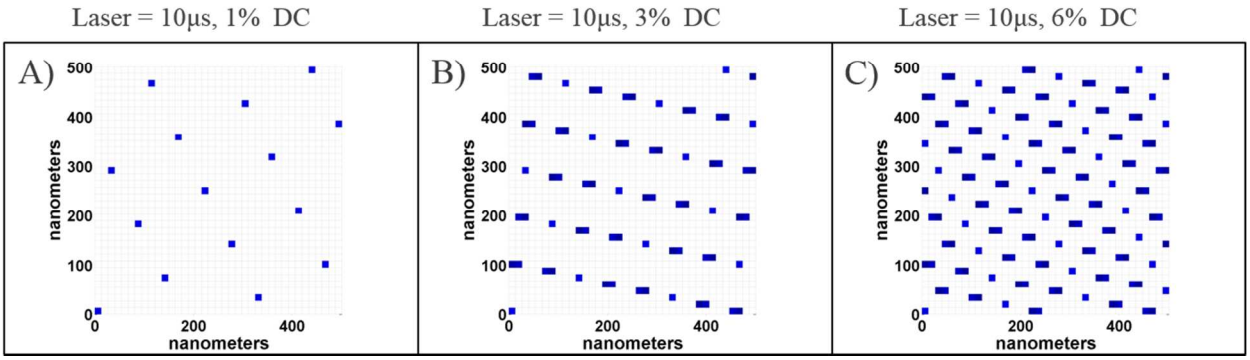


**Figure S2.** Synchronization map of electron beam and laser pulses during the reactive gas assisted LAEBID process. EBID patterns were deposited using a raster scan. The beam scanning initiates in the bottom left corner and terminates at the top right corner. Pixel spacing of the electron dwells are 13.55 nm in the x and y direction. A blue pixel indicates that the electron beam and laser are both simultaneously on and importantly the laser is irradiating the entire box whereas the electron is addressing only single pixels. A white pixel indicates that the laser is off during the 10 µs electron beam dwell on that pixel. The synchronization is shown for LAEBID with 10 µs laser pulses at (A) 1%, (B) 3%, and (C) 6% duty cycles.

**Table S1.** Details and parameters of various LAEBID patterns.

| Laser Conditions | | Gas Conditions | | Electron Beam Conditions | | | | | | |
|---|---|---|---|---|---|---|---|---|---|---|
| **Pulse Width (µs)** | **Duty Cycle (%)** | **Inert Gas** | **Precursor Gas** | **Beam current (pA)** | **Beam energy (keV)** | **Dwell (µs)** | **Refresh (ms/Ebeam Pass)** | **Laser pulses per LAEBID pass** | **Laser On/ Ebeam On (per pixel)** | **Platinum Content (at%)** |
| 100 | 0.1 | Ar | $MeCpPtMe_3$ | 98 | 5 | 10 | NONE | 0.14 | 1.36 | 27.3 |
| 100 | 0.1 | Ar | $MeCpPtMe_3$ | 98 | 5 | 10 | 13.6 | 0.14 | 1.36 | 35.1 |
| 100 | 0.3 | Ar | $MeCpPtMe_3$ | 98 | 5 | 10 | NONE | 0.41 | 4.08 | 29.9 |
| 100 | 0.5 | Ar | $MeCpPtMe_3$ | 98 | 5 | 10 | NONE | 0.68 | 6.81 | 34.5 |
| 100 | 0.5 | Ar | $MeCpPtMe_3$ | 98 | 5 | 10 | 13.6 | 0.68 | 6.81 | 85.3 |
| 10 | 1 | Ar | $MeCpPtMe_3$ | 98 | 5 | 10 | NONE | 13.62 | 13.62 | 24.7 |
| 10 | 3 | Ar | $MeCpPtMe_3$ | 98 | 5 | 10 | NONE | 40.85 | 40.85 | 29.9 |
| 10 | 6 | Ar | $MeCpPtMe_3$ | 98 | 5 | 10 | NONE | 81.70 | 81.70 | 44.3 |

## LCVD

Figure S3a displays a LAEBID pattern deposited with synchronized 100 µs pulse width and 0.5% duty cycle laser pulses. Clearly, island thin film growth was initiated peripheral to the area patterned by the electron dictated 1st half reaction. This peripheral island growth is attributed to contributions from LCVD which are not prevalent at milder laser conditions. Previous simulations[2] suggest that the $SiO_2$ substrate reaches a surface temperature of approximately 300°C, which is similar to common substrate temperatures for Pt CVD and ALD processes[3–5]. Figure S3b displays an EDS spectrum for the LCVD region. There is no distinguishable carbon peak in the spectrum, as the slight low energy peak can be attributed to the Pt-N EDS peak. Thus we conclude that the reactive gas contributes to the CVD process and these conditions realize a simple pyrolytic dissociation of the precursor molecule. The onset of LCVD provides a temperature limitation for the LAEBID process. Specifically, the laser pulses must supply enough photothermal heat to facilitate the purification reaction of the amorphous carbon in the deposit, while remaining below the temperature threshold for the onset of LCVD platinum. A pulsed gas strategy, as opposed to gas co-flow, enables the use of laser conditions that are otherwise not feasible for the reactive gas assisted LAEBID process.

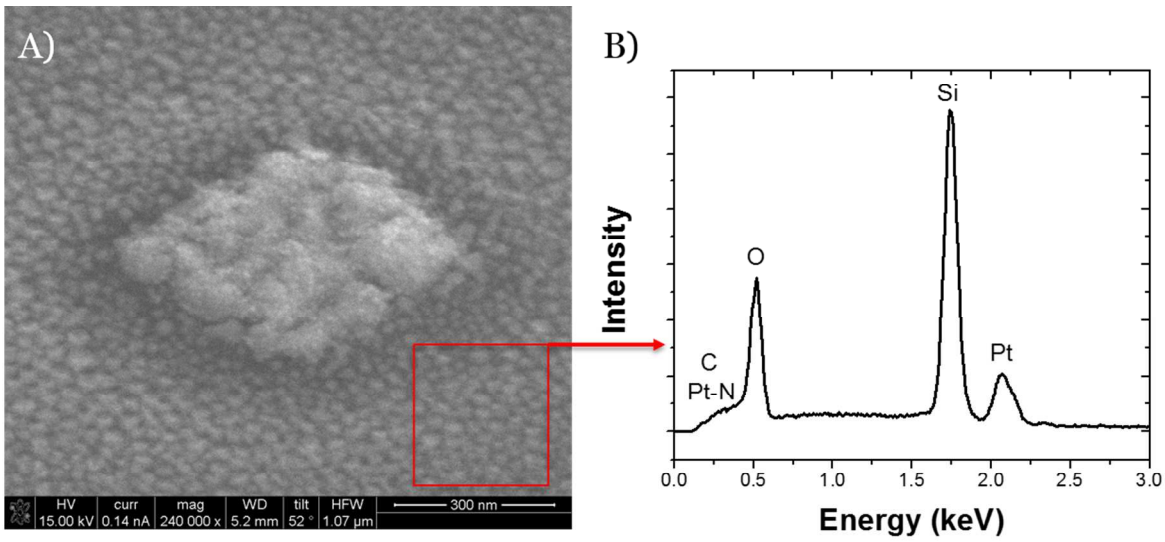


**Figure S3.** (A) SEM image of LAEBID pattern deposited with 100 µs pulse width and 0.5% duty cycle synchronized pulsed laser. Island growth surrounding the deposit was induced by laser assist chemical vapor deposition (LCVD) of the precursor and reactive gas co-flow. (B) EDS spectrum of the LCVD platinum.

**Sequential or layer-by-layer EBID details**

Figure S4a-c displays images of patterns deposited using the cyclic deposition technique with a different number of EBID monolayers deposited per cycle. This technique used a pulsed gas strategy where, (1) precursor gas was injected into the chamber for the electron beam dictated deposition 1$^{st}$ half-reaction, (2) the precursor was subsequently pumped from the chamber and Ar inert gas was injected, and (3) diffusion enhanced residual $H_2O$ molecules facilitate the laser pulse dictated purification 2$^{nd}$ half-reaction. From these images (and complimentary EDS spectra, Fig. S4d), it is clear that the process succeeds in depositing a controllable number of monolayers per cycle with high purity. This provides an extra degree of freedom over typical surface reaction limited ALD processes. Since multiple monolayers can be deposited per cycle with this cyclic deposition technique, the process time required for deposition of a purified pattern can be drastically reduced. However, thicker deposition per cycle can have adverse effects on the deposit's uniformity and smoothness, as is clear by comparing Figures S4a and S4c. It is worth noting that the peripheral deposition seen surrounding the deposits can be

minimized by careful selection of electron beam parameters[6], and the growths on top of deposits in Figures S4a and S4c are a result of an electron beam scanning artifact; neither of these issues are implicit with the cyclic deposition process in general. Converse to Fig. 9, these patterns were deposited using a 5 keV beam energy, instead of 30 keV. This is responsible for the extensive peripheral or proximity deposition shown here.

Smoothing pulses were used after each cycle of the sequential deposition process to reduce the porosity of the deposits. A deposit before and after twenty 100 μs smoothing pulses were applied is displayed in Figures S5a and S5b, respectively. The smoothing pulses allow coalescence of the porous microstructure into a more continuous and smooth microstructure.

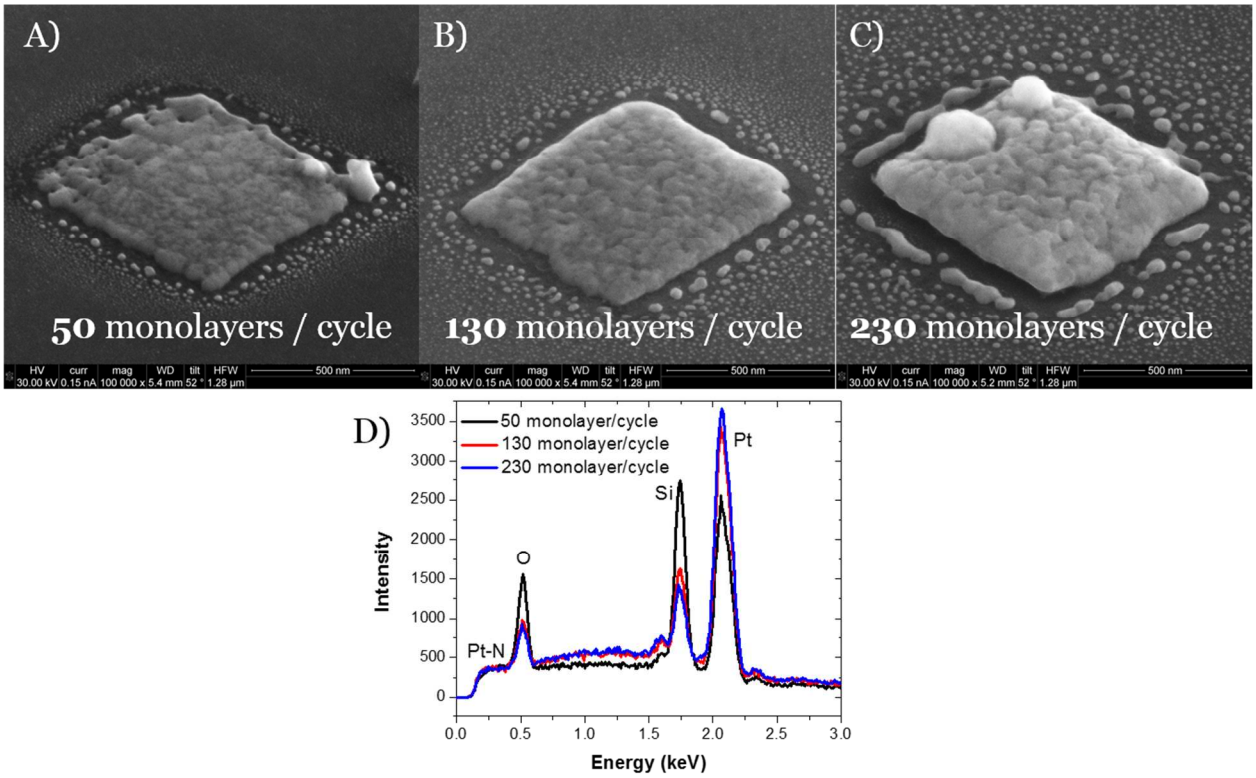


**Figure S4.** Images of patterns deposited using the cyclic deposition technique with (A) 50, (B) 130, and (C) 230 monolayers per cycle. Each pattern was deposited using a total of 6 cycles. (D) EDS spectrum the 130 monolayer/cycle deposit.

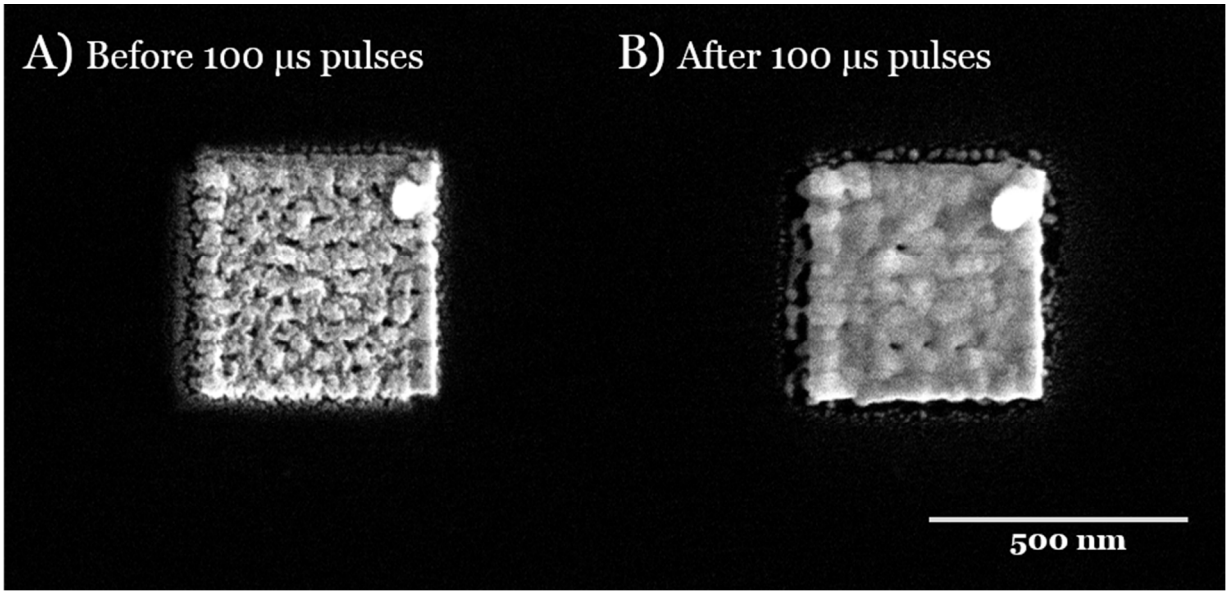


**Figure S5.** Patterns deposited using the sequential method (a) before and (b) after twenty 100 µs laser smoothing pulses were applied.

(1) Geier, B.; Gspan, C.; Winkler, R.; Schmied, R.; Fowlkes, J. D.; Fitzek, H.; Rauch, S.; Rattenberger, J.; Rack, P. D.; Plank, H. Rapid and Highly Compact Purification for Focused Electron Beam Induced Deposits: A Low Temperature Approach Using Electron Stimulated H2O Reactions. *J. Phys. Chem. C* **2014**, *118*, 14009–14016.

(2) Stanford, M. G.; Lewis, B. B.; Noh, J. H.; Fowlkes, J. D.; Roberts, N. A.; Plank, H.; Rack, P. D. Purification of Nanoscale Electron-Beam-Induced Platinum Deposits via a Pulsed Laser-Induced Oxidation Reaction. *ACS Appl. Mater. Interfaces* **2014**, *6*, 21256–21263.

(3) Kwon, J. H.; Yoon, S. G. Characterization of Pt Thin Films Deposited by Metallorganic Chemical Vapor Deposition for Ferroelectric Bottom Electrodes. *J. Electrochem. Soc.* **1997**, *144*, 2848–2854.

(4) Knoops, H. C. M.; Mackus, A. J. M.; Donders, M. E.; van de Sanden, M. C. M.; Notten, P. H. L.; Kessels, W. M. M. Remote Plasma ALD of Platinum and Platinum Oxide Films. *Electrochem. SOLID STATE Lett.* **2009**, *12*, G34–G36.

(5) Aaltonen, T.; Ritala, M.; Tung, Y. L.; Chi, Y.; Arstila, K.; Meinander, K.; Leskela, M. Atomic Layer Deposition of Noble Metals: Exploration of the Low Limit of the Deposition Temperature. *J. Mater. Res.* **2004**, *19*, 3353–3358.

(6) Arnold, G.; Timilsina, R.; Fowlkes, J.; Orthacker, A.; Kothleitner, G.; Rack, P. D.; Plank, H. Fundamental Resolution Limits during Electron-Induced Direct-Write Synthesis. *ACS Appl. Mater. Interfaces* **2014**, *6*, 7380–7387.